# See through Disaster Rubble in 3D with Ground Penetrating Radar and Interactive Augmented Reality for Urban Search and Rescue

Da Hu[1], S.M.ASCE; Long Chen[2], Ph.D. A.M.ASCE; Jing Du[3], Ph.D. M.ASCE; Jiannan Cai[4], Ph.D. A.M.ASCE; Shuai Li[5,*], Ph.D. A.M.ASCE

[1] Department of Civil and Environmental Engineering, The University of Tennessee, Knoxville, TN 37996, USA. Email: dhu5@vols.utk.edu

[2] School of Architecture Building and Civil Engineering, Loughborough University, Loughborough LE11 3TU, UK. Email: l.chen3@lboro.ac.uk

[3] Engineering School of Sustainable Infrastructure & Environment, University of Florida, Gainesville, FL 32611, USA. Email: eric.du@essie.ufl.edu

[4] Department of Construction Science, The University of Texas at San Antonio, San Antonio, TX 78207, USA. Email: jiannan.cai@utsa.edu

[5] Department of Civil and Environmental Engineering, The University of Tennessee, Knoxville, TN 37996, USA. Email: sli48@utk.edu

* Corresponding Author, Shuai Li, Email: sli48@utk.edu

**Abstract**

First responders often lack information and visual clues regarding interior spaces in disaster rubble, preventing efficient, effective, and safe search and rescue for victims trapped in collapsed structures. Rapidly detecting and acquiring information about the voids in collapsed structures that could contain surviving victims is critical for urban search and rescue. However, reconstructing the buried voids in three-dimension (3D) and communicating the relevant information such as buried depth and void size to first responders remain a significant challenge. To address this challenge, this study proposes a see-through technique by integrating ground penetrating radar (GPR) with interactive augmented reality (AR). The contribution of this study is two-fold. First, a new method is developed to process collected GPR data to reconstruct potential voids in disaster rubble in 3D and extract the buried depth and void size from the GPR data. The coordinates of void boundaries are extracted from multiple GPR scans to generate sparse point

clouds. An improved alpha shape method is exploited to reconstruct the 3D space beneath disaster rubbles from the point clouds. Second, an interactive augmented reality interface is developed to enable first responders to visualize the voids in collapsed structures in 3D together with relevant information to assist urban search and rescue. The results from simulations and pilot experiments demonstrate the feasibility and potential of the proposed methods.

**Keywords**

Augmented Reality; Ground Penetrating Radar; Urban Search and Rescue; Subsurface Reconstruction; Disaster

## Introduction

Natural and man-made disasters result in massive structural collapses, and searching and rescuing survivors from collapsed structures remain a significant challenge. According to Murphy et al. (2001), 15% of victims were found to be trapped in void spaces beneath collapsed structures. Searching for trapped victims is a fight against time, as their survival rate falls considerably after two days (Murphy et al. 2001). First responders are the main force to search the trapped victims in void spaces, and the success largely relies on their situational awareness regarding the survivable void spaces in collapse structures. The types of voids are typically divided into four categories that are V shape, A-frame, pancake, and lean-to voids (Poteyeva et al. 2007). Among them, lean-to collapse void is the most common at disaster sites (Couch 2008). The trapped victims have a higher survivable rate in lean-to void because it forms a large survivable void space, known as “triangle of life”. The conventional methods to locate the voids in disaster rubble are based on first responders’ field observation from the surface. Relying on the experience of first responders, this method cannot provide quantitative information regarding the interior void spaces. To address this limitation, Building Information Modeling (BIM) is combined with a collapse simulation engine to simulate different damage patterns of the building, which compiles a damaged database (Bloch et al. 2016). The as-damaged exterior model is then compared with the database to select the closest match solution in the database. The void space in the collapsed building is then predicted using the candidate solution. However, the method requires a BIM model of the damaged building before the earthquake, which cannot be obtained for most of the buildings. In addition, the validity of simulation engines is questionable for complex building structures in the real world.

There is a critical need to reconstruct void spaces in disaster rubbles, and visually communicate the relevant information to first responders to ensure safe, efficient, and effective search and rescue. The absence of a solution to this need represents an important problem because unguided search and rescue operations may waste valuable time and effort to rescue victims and put first responders at risk. Search and rescue operations can be significantly improved, if first responders can continuously "see" the occluded spaces through heterogeneous disaster rubble and be aware of the critical voids that may contain trapped victims. Therefore, this study proposes a novel framework to see through disaster rubbles in 3D by integrating airborne ground penetrating radar (GPR)-based sensing for void reconstruction and augmented reality (AR) interface for information communication. Ground Penetrating Radar (GPR) is used to detect and reconstruct potential void spaces beneath disaster rubbles. The reconstructed void information including geometry, volume, and buried depth are communicated to first responders through the AR interface.

This research leads to a new framework that integrates an unmanned aerial vehicle (UAV)-borne GPR system to obtain information regarding voids in disaster rubbles and an AR-based interface to communicate void information to first responders for search and rescue. The contribution of this research is two-fold. First, a new method is proposed to detect void boundaries from GPR scans and estimate the coordinates based on the detected boundary with first responders in the loop. An improved weighted alpha shape method is then used to reconstruct voids in rubbles using the boundary coordinates, and therefore detailed information including void size and depth can be retrieved. Second, an AR-based interface is developed to communicate the void information to first responders, providing them important situational awareness and contextual guidance on disaster sites. Hence, the proposed methods have the potential to improve the traditional experience-based search and rescue practice to an information-based paradigm.

## Literature Review

### *Related Studies on GPR in search and rescue*

GPR is a non-destructive technique that has been widely used in subsurface mapping and demonstrated to be an effective method. A large and growing body of literature has developed methods to detect and locate subsurface targets, such as underground utility (Cai et al. 2020; Li et al. 2015; Yuan et al. 2018), crack (Levatti et al. 2017; Tong et al. 2017), root (Aboudourib et al. 2019; Hu et al. 2020b; Liu et al. 2020b), concrete rebar (Hu et al. 2020a), and tunnel (Núñez-Nieto et al. 2014). Table 1 summarizes related studies on GPR applications in the search and rescue domain, including avalanche victim detection, victim detection, and void detection in collapsed rubbles.

Table 1 Related studies on GPR in search and rescue.

| Application | Approach | Limitations | Reference |
|---|---|---|---|
| Avalanche victim detection | Recognize hyperbola signal caused by buried victims | Cannot adapt to collapsed buildings due to a more complex scenario than an avalanche | (Fruehauf et al. 2009; Heilig et al. 2008) |
| Victim detection under collapsed rubbles | Monitor human respiration and movement | Require the GPR to be in proximity of victims which is hard to obtain without knowing subsurface conditions. | (Cist 2009; Liu et al. 2014; Yan et al. 2021; Yang et al. 2019) |
| Void detection under collapsed rubbles | Recognize boundary features from radargram | Cannot provide void boundary coordinates and void volume | (Chen et al. 2020; Hu et al. 2019) |

**Avalanche victim detection**. GPR mounted on the helicopter has been used to detect avalanche victims for decades. For example, Heilig et al. (2008) conducted a feasibility study of GPR in avalanche victim detection. In particular, Heilig et al. (2008) investigated the influence of snow properties on radar signal, the maximum horizontal distance of a buried victim from the flight direction, and the influence of the scanning direction. In their study, they also developed a semi-automatic detection algorithm to recognize potential victims from GPR scans. The method is dependent on a handcrafted snowpack extraction to remove the zone of air and underground in the radargram. To address this limitation, Fruehauf et al. (2009) developed an automated real-time detection of avalanche victims using airborne GPR. Their method utilized an active contour model to automatically extract snowpack. Thereafter, a matched filter method was used to detect hyperbola, which is believed to be the signal feature of buried victims in the radargram.

However, detecting victims in structural collapses are more challenging than that in avalanche snowpack, because structural collapses are always cluttered and heterogeneous.

**Victim detection under collapsed structures**. A number of studies have examined the Ultra-wideband (UWB) GPR in victim detection under collapsed structures. The UWB GPR exhibits very fine range resolution due to its large bandwidth, which can capture target features that are much smaller than the target size. For example, in (Cist 2009), UWB GPR was used to detect survivors' motion and breathing in rubble piles by leaving the antenna stationary. Liu et al. (2014) conducted a numerical simulation to investigate human vital sign detection under collapsed structures caused by earthquakes using UWB GPR. The collapsed structure was simulated according to site conditions with two entrapped victims. In their study, source separation and empirical mode decomposition were proposed to locate human subjects in the recorded radargram. Yang et al. (2019) proposed a novel method to identify and locate human vital signs from radar-received signals based on permutation entropy (PE) and ensemble empirical mode decomposition (EEMD) algorithm. In a more recent study, Yan et al. (2021) designed a novel Golay complementary coded system to detect quasi-static trapped victims under collapsed structures. The proposed system can detect non-periodic strong respiration with stationary operating mode and quasi-periodic weak respiration pattern using scanning operating mode. While these methods have been demonstrated to be feasible and applicable in detecting victims under rubbles, the success of victim detection is based on the premise that the victims are in close proximity to the GPR, which is difficult to achieve without knowing subsurface conditions. Identifying subsurface survivable void in disaster rubbles can pinpoint locations with potential victims, and thus facilitating such victim detection methods.

**Void detection under collapsed structures**. More recent attention has focused on detecting void space under collapsed structures to pinpoint areas with potential entrapped survivors. For instance, In (Hu et al. 2019), a probabilistic-based algorithm was developed to detect void boundary in GPR scans for lean-to collapse void. The method was demonstrated to be effective to detect void boundary in the radargram for simplified lean-to collapse void. In (Chen et al. 2020), GPR is mounted at the bottom of the drone to locate critical void space under the rubble to save trapped victims. However, these existing methods have not leveraged boundary features to extract their coordinates and combined multiple GPR scans for 3D reconstruction. This study aims to address this knowledge gap.

***Related Studies on Augmented Reality in Search and Rescue***

Augmented Reality (AR) technology can be a powerful tool to communicate context-aware information, as it can intuitively present virtual content in the real world. AR technology has been used to support disaster search and rescue in a variety of ways, such as robot control and interaction, commander and responder collaboration, and point-of-interests (POI) information visualization. Table 2 summarizes the related studies on AR in search and rescue.

Table 2 Related studies on augmented reality in search and rescue.

| Application | Registration method | Limitations | Reference |
|---|---|---|---|
| Robot control and interaction | Marker-based; NA | Require marker to be installed; cannot align virtual information at disaster sites | (Burian et al. 2014; Coovert et al. 2014; Gianni et al. 2013; Reardon et al. 2018) |
| Commander and responder collaboration | | | (Bacim et al. 2012; Vassell et al. 2016; Wani et al. 2013) |
| Point-of-interest (POI) visualization | Location-based | May fail to register virtual information in crowded urban areas | (Campos et al. 2019; Wang et al. 2018) |

**Robot control and interaction**. Many studies have developed interfaces to facilitate human-robot coordination in search and rescue (SaR) using AR technology (Burian et al. 2014; Coovert et al. 2014; Gianni et al. 2013; Reardon et al. 2018). For instance, in (Burian et al. 2014), an AR-based user interface was developed to control a fleet of robots including unmanned ground robots (UGV) and unmanned aerial robots (UAV). With the interface, operators have the flexibility to control multiple robots and conduct search and rescue missions at the same time. Coovert et al. (2014) studied communication strategies to convey robot upcoming movements to humans. An augmented reality projection system is proposed to communicate robot intended movement to humans via visual arrows and a simplified map. Reardon et al. (2018) developed an AR system that enables cooperative search between human and robot teams. Through the AR device, the robot can share search results with human teammates. In addition, this AR interface can provide a navigation route to first responders and let them reach their desired target efficiently.

**Commander and responder collaboration**. A variety of studies have utilized AR to facilitate collaboration between incident commanders and responders in search and rescue operations. For example, AR was used in a collaborative guidance system after disasters for search and rescue in a complex building (Bacim et al. 2012). The system allows incident commanders and first responders to communicate with each other effectively using visual and nonverbal information when searching a disaster site. Vassell et al. (Vassell et al. 2016) developed a novel intelligent dashboard for an AR-based coordination system for multiple incidents. The system integrated Incident Command System (ICS) with the Internet of Things (IoT) to achieve minimal human communication and thus improve coordination efficiency. In (Wani et al. 2013), a wearable AR system was developed to improve collaboration among different agencies using hand gestures. This method was applied and demonstrated in a fire emergency scenario. However, all of the above-mentioned approaches either required markers to register virtual information or didn't utilize the registration method, which cannot accurately align void information on collapsed structures at disaster sites.

**POI information visualization**. A recent study conducted by Wang et al. (2018) designed an AR system to mark the target of interest and then display the target information on the screen of the AR device. In addition, the system can display the target even when it is outside the view of the camera. Campos et al. (2019) developed a location-based augmented reality application to provide insight into the surrounding through mobile phones to improve their situational awareness. The responders can also exchange information using the application to increase SaR efficiency. However, these two studies are location-based AR, which requires a high-level positioning accuracy. In urban search and rescue, it is difficult to achieve accurate positioning. Our study aims to address this knowledge gap by utilizing image-based AR, which is suitable for complex disaster scenes.

## Methodology

Fig. 1 presents an overview of the framework to integrate GPR-based 3D void reconstruction and AR visualization. In the first step, the UAV-borne GPR system is used to survey disaster sites and collect image and GPR data. The fast-moving speed of the UAV enables first responders to survey disaster sites quickly and efficiently. The integration of UAV and GPR can be used to survey structural collapses that are dangerous or inaccessible. In the second step, void boundary coordinates are estimated in multiple scans to generate a sparse 3D point cloud. Thereafter, an improved weighted alpha shape algorithm is proposed to generate a 3D model of void space using the sparse point cloud. The third step develops an AR interface to communicate void information such as the buried depth and volume of a void to first responders. The image-based registration approach is adopted to register void information on disaster sites.

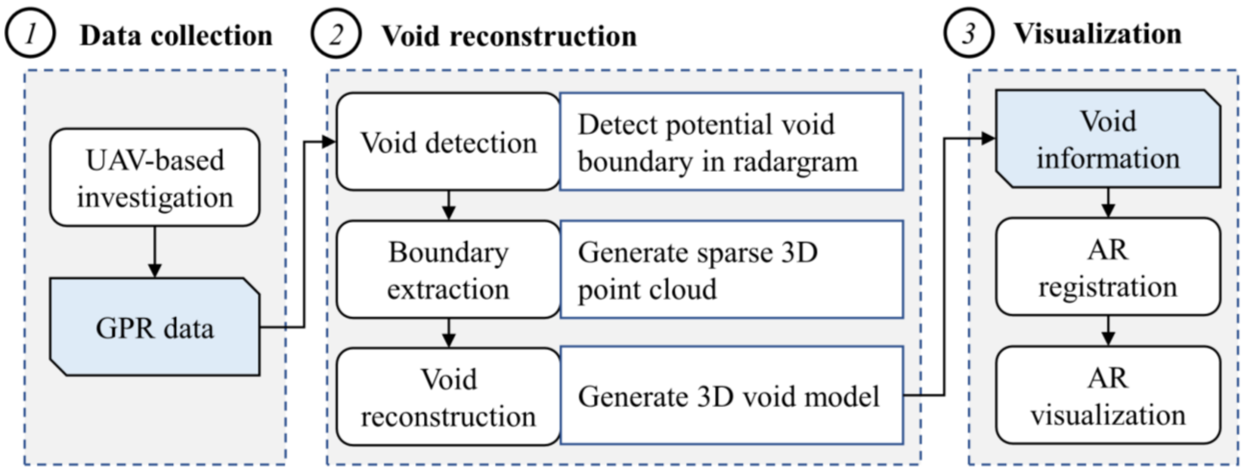


**Fig. 1**. Methodology overview

### ***System Configuration and GPR Data Collection***

The UAV is equipped with a real-time kinematic (RTK) global positioning system (GPS), inertial measurement unit (IMU), camera, and GPR. RTK GPS can provide centimeter-level positioning accuracy for the UAV, which is an essential component to acquire spatial position information. RTK GPS can also provide accurate positioning for GPR and image data. IMU measures the orientation, velocity, and gravitational forces of the UAV to aid navigation and control. The camera is used to capture surrounding information of the disaster area and collect video data. The video stream gives the first responder the ability to search disaster areas from a bird's view. In addition, images are also collected for structural collapses, which will be used as the target to register void information in the real world. GPR mounted on the UAV can detect subsurface structures such as buried void space under rubbles. GPR is a geophysical method that uses high-frequency radio waves to image the subsurface. Specifically, GPR transmits high-frequency EM waves into the ground and receives reflected signals when the energy encounters boundaries with different materials such as void boundaries. The reflected signal strength is determined by the relative permittivity contrast between two materials. The higher the contrast, the reflected signal will be stronger. The void boundary is the interface between collapse structures formed by typical building material and void formed by air. The relative permittivity of air is 1 and 3-10 for common building materials such as concrete and brick (Zhekov et al. 2020). The large permittivity contrast will lead to strong reflections at the interface, which is an important feature to determine the void boundary.

The UAV can be teleoperated by a first responder to survey disaster areas following a disaster. The first responder can recognize structural collapses from video data stream and locate the rubble with a high probability of void based on two observations. First, the lean-to collapse void occurs when one side of a building fails and stays anchored at the other end, creating a large triangular void. Second, the integrity of large building components to some extent is preserved, which implies the continuity of their geometries under occlusions. Thereafter, the first responder can control the UAV to fly toward the rubble. When approaching the rubble, the first responder will lower the altitude of the UAV and capture the rubble surface image. The image will be used to link the information of surface disaster rubble and subsurface voids reconstructed from GPR data. When arriving at the rubble, the first responder will determine appropriate GPR scanning trajectories given site conditions. For lean-to collapse void, the UAV will fly along the slope of the lean-to collapse structures. In this way, topographic effects on GPR data can be reduced, given the variation of ground surface elevation will affect the propagation of EM waves. In addition, the altitude of the UAV is controlled within 3m to reduce the GPR signal loss in the zone of air above ground. This is because the GPR signal suffers from energy loss due to geometrical spreading, and a lower amplitude penetrates through the subsurface could lead to a weaker reflection amplitude from the void boundary that becomes hard to recognize. Therefore, the altitude of the UAV should maintain within a certain range to reduce energy loss in the air. This can be achieved coincidently with the UAV scanning trajectory because the UAV is generally equipped with Radar and Lidar altimeter to measure its distance from the ground. Fig. 2 illustrates the GPR survey of a lean-to collapse void using the UAV-borne GPR system and the corresponding GPR B-scan. The B-scan in the figure is simulated using the gprMax simulator (Warren et al. 2016a) with a 900MHz antenna.

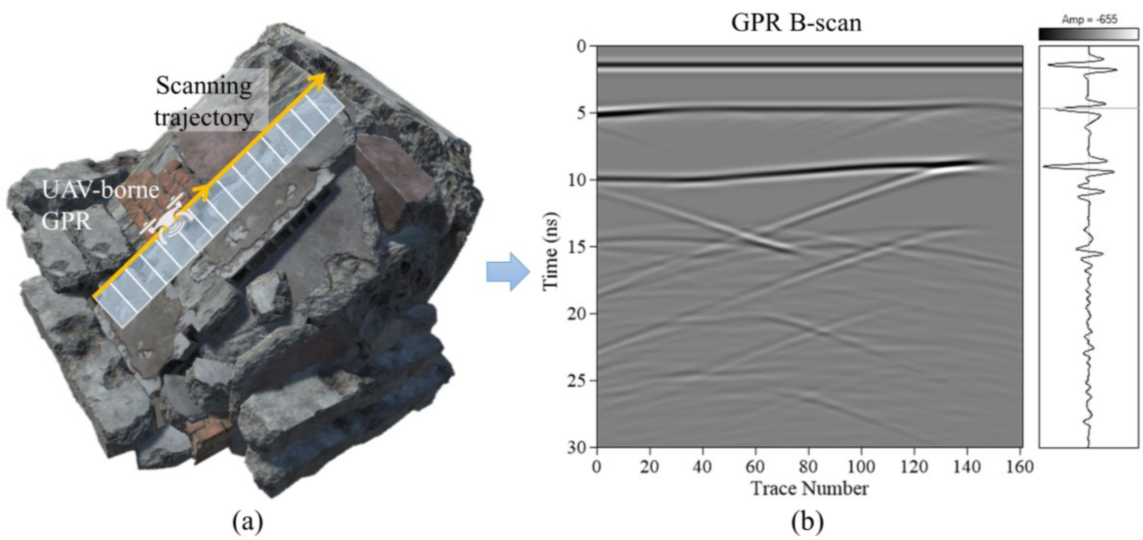


**Fig. 2**. Illustration of the GPR survey of a lean-to collapse void: (a) UAV-borne GPR survey along lean-to collapse rubbles; and (b) GPR B-scan

***Void reconstruction***

The 3D reconstruction of void using GPR scans consists of two steps. In the first step, void boundary coordinates are extracted to form a sparse 3D point cloud. The second step proposes an improved weighted alpha shape (WAS) method to reconstruct the 3D model using the processed point cloud.

*Void Boundary Detection*

After the UAV surveying, first responders will process the GPR data for each structural collapse. The void boundary needs to be extracted in the radargram to estimate boundary coordinates. The lean-to collapse forms a triangular void space known as “triangle of life”, which is supported by floor and wall to maintain its structural stability. The geometric configuration of lean-to collapse will lead to a triangular zone in the radargram formed by void boundary features. The boundary features represent reflections from the interface between void and rubbles, the interface between void and floor, as well as interface between void and wall. First responders will leverage boundary features and their triangular relationship to determine the existence of void. The void boundary consists of upper and lower boundaries. The upper boundary is the reflection from the interface between collapsed rubbles and void. The lower boundary is composed of reflection from both the floor and the wall. In addition to the void boundary, ground reflection also needs to be extracted to calculate coordinates of void boundary, which is the first significant reflection recorded in the radargram.

A semi-automatic approach is developed to detect void boundaries and ground reflection in the radargram, which consists of three steps. First, deep learning (DL)-based edge detection method is adapted to extract edge features in the radargram (Wibisono and Hang 2021). This is because the ground surface and void boundary have relatively strong reflections due to the large dielectric constant contrast with air. The edge detection model is trained on BSDS500 and PASCAL VOC 2012 datasets, which are standard benchmarks for edge detection in images. Second, OTSU's thresholding method (Otsu 1979) is used to further refine detected edges using the DL-based method, and convert edges into binary classes (i.e., boundary and non-boundary). OTSU is an automatic binarization level decision approach based on the shape of the histogram of pixel intensities. The interface also provides a double thresholding alternative option to the user by setting a high and low threshold manually. Third, based on the detected boundary, first responders can annotate the void boundary in the radargram with their judgment. An interactive interface is developed to facilitate the boundary annotation process. The interface can process multiple radargrams at the same time. Fig. 3 shows an implementation of the method in the interface.

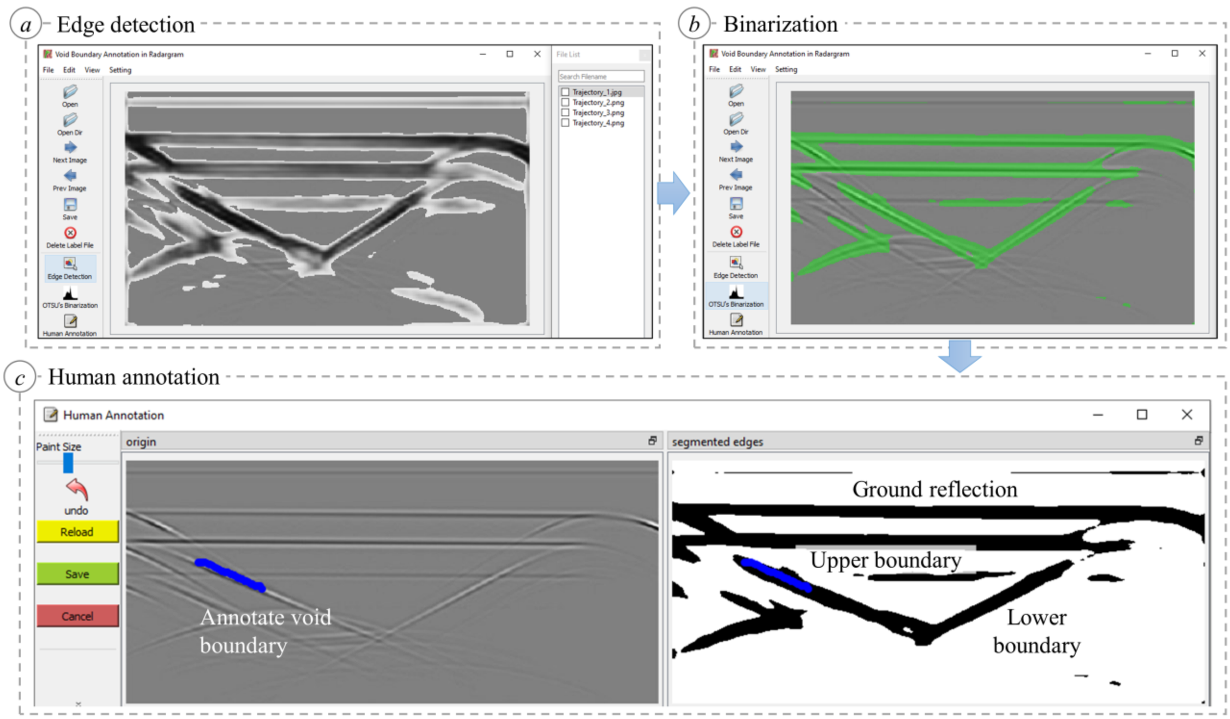


**Fig. 3.** Void boundary annotation interface: (a) edge detection; (b) binarization; and (c) human annotation

*Void Boundary Coordinates Estimating*

To estimate coordinates of void boundary segmented in the radargram, we make three simplifying assumptions shown below.

**Assumption 1**. The covered rubble layer of the lean-to collapse void is assumed to be homogeneous. The research conducted by (Li et al. 2020; Liu et al. 2020a; Zhang and Hoorfar 2019) also adopted this assumption for subsurface layers. In our study, the developed method is still in its initial stages, which aims to demonstrate the feasibility of GPR-based reconstruction for lean-to collapse structures.

**Assumption 2**. The wave is transmitted in an arc shape and the center is the tangent point of incident EM wave on the interface between covered rubble and void, when the EM wave transmits into a medium with much smaller relative permittivity. Appendix A shows the proof for this assumption.

**Assumption 3**. The objects such as furniture inside a lean-to collapse void are treated as a part of the void. This assumption aims to avoid underestimating the volume of void in collapsed structures that may contain survivors.

The void boundary coordinates need to be extracted for 3D reconstruction. Fig. 4 illustrates a schematic diagram of the UAV survey at the transition point. The transition point represents the void lower boundary reflection changes from the floor to the wall. The coordinate of UAV is G (x, y, z) which can be obtained from on-board RTK-GPS. The EM wave first travels through the air and reaches the surface of collapsed rubbles. GP is perpendicular to the surface of the rubble since it is the shortest path from the UAV to the ground. The reflection from the surface is the first significant reflection recorded in the radargram, which can be easily recognized. Then, the EM wave penetrates through the rubble and arrives at the upper boundary of the void. For a lean-to collapse void, the surface of the rubble can be considered to be parallel with the void upper boundary. As such, the ray paths GP and $PV_U$ can be viewed in the same direction. The reflection from the void upper boundary is the first continuous strong reflection that appears below the surface reflection in the radargram.

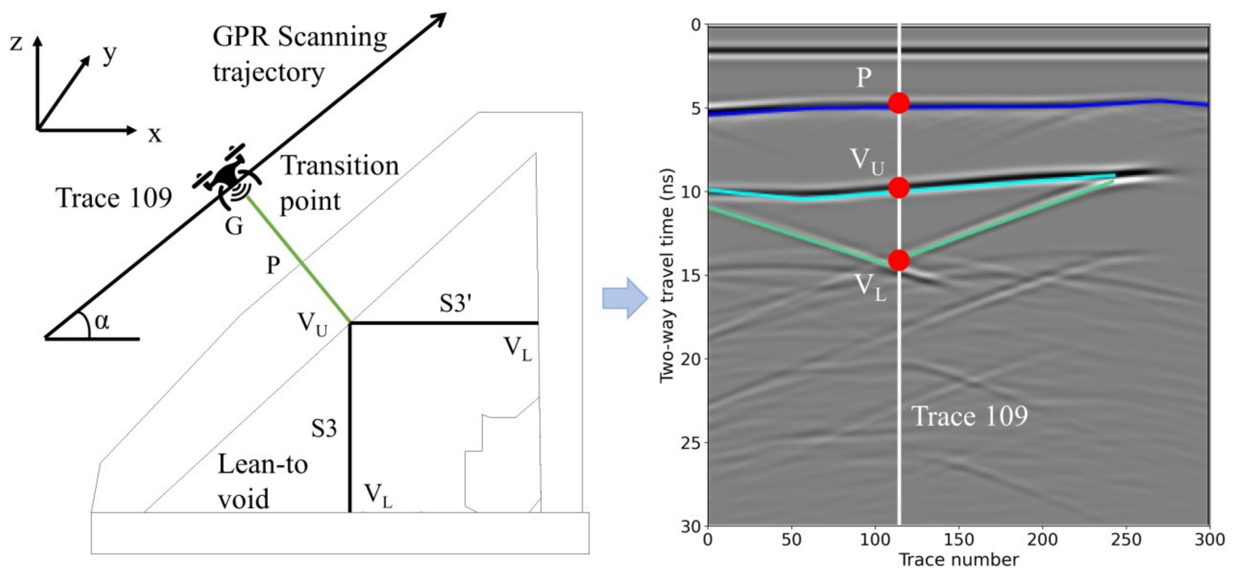


**Fig. 4**. Schematic diagram of UAV survey at the transition point

Finally, the EM wave travels in the void space and reaches the floor or the wall. Note that floor and wall support for lean-to collapsed void are generally horizontally and vertically laid out, respectively. According to Assumption 2, the ray path $V_UV_L$ that is perpendicular to the floor or the wall has the shortest travel distance, which is assumed to be first reflected in this study. The detected lower boundary in the radargram consists of reflection from both the floor and the wall. The left section of the lower boundary is the reflection from the floor and the right section comes from the wall. The transition point can be obtained from the detected boundary, which is the trace with the largest travel time on the lower boundary. When the UAV is at the transition point, the distance from $V_U$ to the floor $S_3$ and the wall $S_3'$ is the same. The reflection will come from the wall section after the UAV passes the transition point.

Fig. 5 shows the schematic diagram of coordinates calculation for floor boundary. The coordinate of upper void boundary for trace *i* is $V_U$ (x', y', z') that can be approximated in Eq. (1), where $S_1$ is the perpendicular distance from the UAV to the ground surface, and $S_2$ is the distance from point P to upper boundary $V_U$, $\beta$ is the upward flying angle of the UAV.

$$\begin{cases} x' = x + (S_1 + S_2)\, sin\, \beta \\ y' = y \\ z' = z - (S_1 + S_2)\, cos\, \beta \end{cases} \tag{1}$$

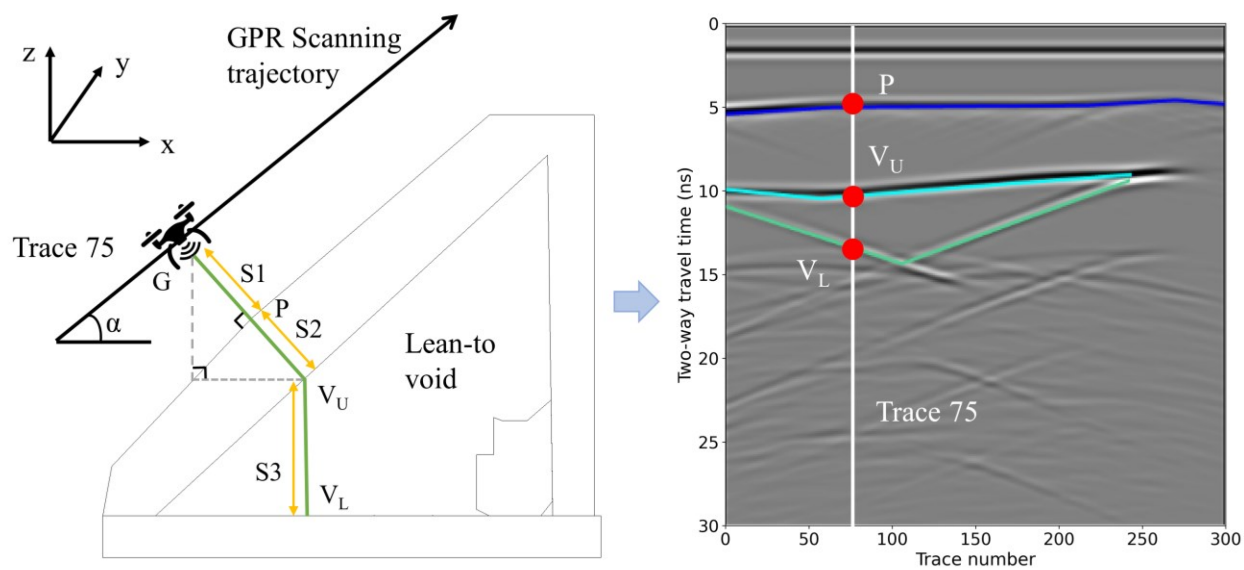


**Fig. 5**. Schematic diagram of coordinates calculation for floor boundary

$S_1$ and $S_2$ can be estimated using collected GPR scans as indicated in Eq. (2), where *c* is the speed of light equals $3\times10^8$ m/s, $t_i$ is the two-way travel time in medium *i* provided by the radargram, $\varepsilon_i$ is the relative permittivity of the material. $S_1$ is the wave travel distance in the air which means $\varepsilon_i$ is 1. $S_2$ is the wave propagation from the rubble surface to the void upper boundary, which can be treated as void depth. Since multiple GPR scans are collected for each structural collapse to reconstruct the void, the buried depth of the void is estimated by an average value of $S_2$. This is because void depth could be different at different locations. This layer consists of typical building materials such as concrete, brick, and wood. The relative permittivity of this layer can be estimated based on the surface condition. For instance, for a collapsed concrete building, the relative permittivity of the rubble layer can be approximated by the concrete material which is around 7.

$$S_i = \frac{ct_i}{2\sqrt{\varepsilon_i}} \tag{2}$$

The coordinate of floor boundary for trace $i$ is $V_L$ (x'', y'', z'') that is calculated in Eq. (3), where $S_3$ represents the distance to the floor from the upper boundary $V_U$.

$$\begin{cases} x" = x + (S_1 + S_2)\sin\beta \\ y" = y \\ z" = z - (S_1 + S_2)\cos\beta - S_3 \end{cases} \tag{3}$$

When the GPR passes the transition point, the reflection on the lower boundary will come from the wall as indicated in Fig. 6. The coordinates of the upper boundary will be calculated using Eq. (1). The coordinate of the lower boundary is given in Eq. (4).

$$\begin{cases} x" = x + (S_1 + S_2)\sin\beta + S_3 \\ y" = y \\ z" = z - (S_1 + S_2)\cos\beta \end{cases} \tag{4}$$

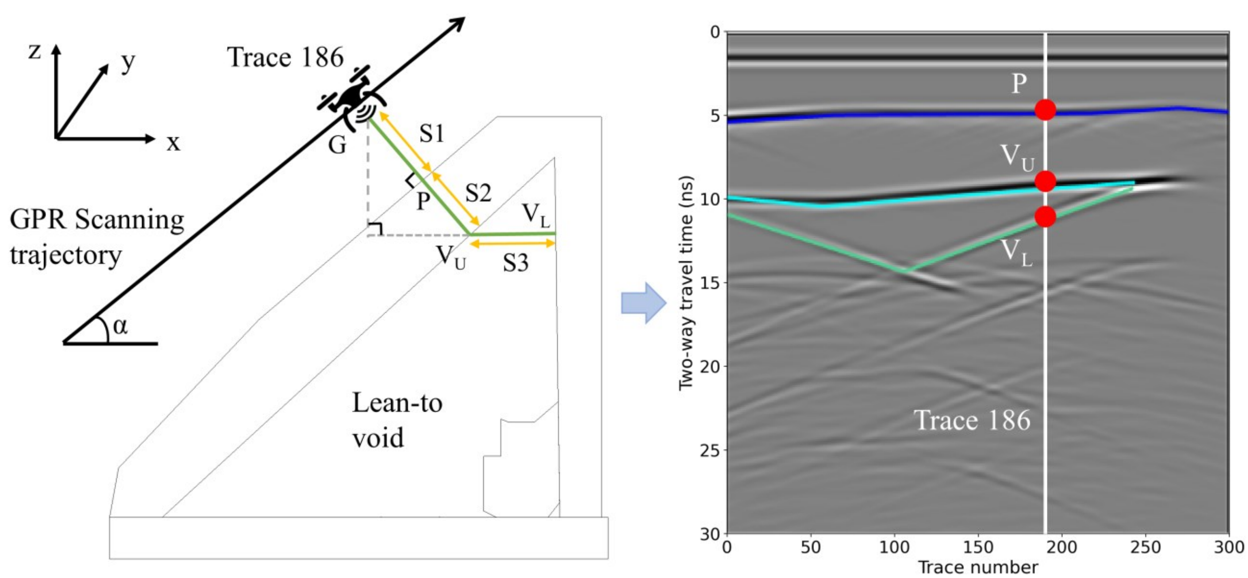

**Fig. 6**. Schematic diagram of coordinates calculation for wall boundary

As indicated in Fig. 4, there will be missing void boundaries on the floor and wall that will not have reflections appear on the detected void boundary in the radargram. The missing detection will lead to an underestimate of void volume. According to Assumption 3, the missing section at the floor and wall is estimated by linearly extrapolating using detected sections as indicated in Fig. 7. The extracted boundary coordinates from multiple GPR scans form a sparse 3D point cloud, which will then be fed to the void reconstruction algorithm.

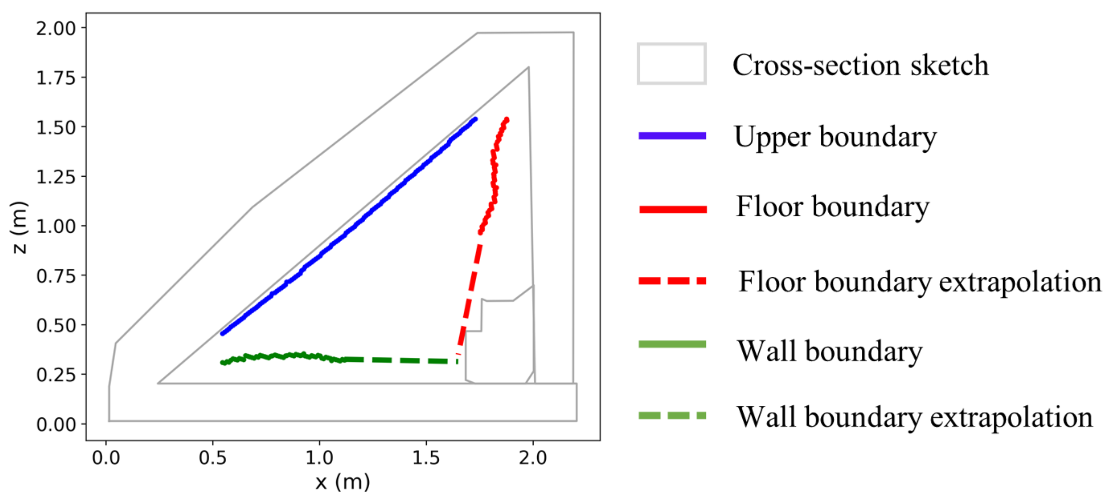


**Fig. 7**. Results of segmented boundary coordinates and extrapolation

*3D Model Generation*

The alpha shape method is selected to reconstruct void space using the sparse 3D point cloud. The method is selected for two main reasons. First, the algorithm has been demonstrated to be fast and effective in 3D reconstruction (Gomes et al. 2014). Second, the method can provide an accurate estimation of the volume (Al-Tamimi et al. 2015). However, for the traditional alpha shape approach, the shape of the reconstructed model is determined by a single $\alpha$ value, which is not suitable for non-uniformly distributed point cloud data. If $\alpha$ value is chosen for dense regions, then the reconstructed model will have holes or beak apart in sparser regions. For instance, the $\alpha$ value can be either too small or too large in some regions if the point cloud is not evenly distributed. To overcome this limitation, a weighted alpha shape (*WAS*) method is developed for void reconstruction. The proposed *WAS* method assigns different weights for each point in the set. The weight is determined by the density of points in the region. The low-density regions have a relatively large weight for the $\alpha$ value. The algorithm is detailed as follows.

1) Determine k nearest neighbors for each point using k-d tree algorithm (Hajebi et al. 2011) given point cloud $\mathbf{P}$ ($p_1$, $p_2$, …, $p_n$); Calculate average distance $\mathbf{d}$ ($d_1$, $d_2$, …, $d_n$) for each point to its nearest neighbors.
2) Draw tetrahedra between points using the Delaunay Triangulation (DT) which can ensure each tetrahedron contains no other points in its interior.
3) Calculate median edge length $L_m$ of tetrahedral mesh.
4) Calculate the radius of the sphere circumscribed about tetrahedron $T_1$. $T_1$ is formed by vertices $p_a$, $p_b$, $p_c$, and $p_d$, which are four points in the point cloud $\mathbf{P}$.
5) Calculate threshold value $\alpha_w$ for $T_1$ using Eq. (5), where $\bar{d}$ is the mean of $\mathbf{d}$ calculated in step 1.

$$\alpha_w = \frac{d_a+d_b+d_c+d_d}{4\bar{d}} \times 2L_m \qquad (5)$$

6) Remove the edges of the tetrahedra if the radius calculated in step 3 is larger than $\alpha_w$; Keep the edges if the radius is smaller than $\alpha_w$.
7) Repeat steps 3-5 recursively until all the tetrahedra are processed.
8) Generate 3D model in STL format using preserved edges.

The parameter *k* determines the number of nearest neighbors for each point. The k is typically selected as the square root of the total number of points (Nadkarni 2016). The α value is set as two times median edge length $L_m$ of tetrahedral mesh to ensure resulting alpha shape enclosing all points with one region. The volume of the 3D model is also estimated based on the discrete form of the divergence theorem (Alyassin et al. 1994). The volume is calculated in Eq. (6), where $z_i$ is the z component of the centroid coordinate, $a_i$ is the triangle area, and $nz_i$ represents the z component of normal of the *i*th triangle.

$$V = \sum_i z_i a_i \, nz_i \qquad (6)$$

Fig. 8 shows a representative result of void reconstruction using the proposed approach. The estimated depth and volume of the reconstructed void are 0.51m and 0.87m$^3$, respectively. The generated void information needs to be communicated to the first responders to improve their situational awareness regarding subsurface void. Next, the development of an AR-based visualization system is presented.

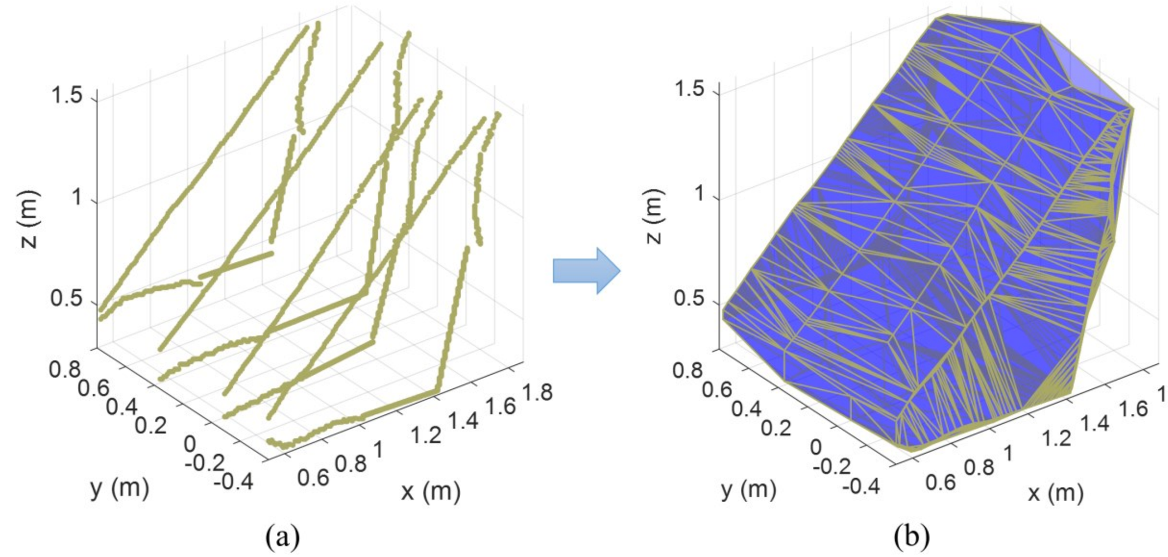


**Fig. 8**. Example of reconstructed void: (a) void boundary coordinates; and (b) reconstructed void

***AR-Based Visualization***

The generated void information is registered to the real world using the image-based approach. Ground surface images are collected during the UAV survey from on-board camera. The image is corresponded to void information beneath the rubbles. A database is established to store void information and image for each structural collapse. The database stores ID, image, 3D void model, void volume, and void buried depth for each site. The images and void information will be uploaded to the database after the UAV finishes the survey. The registration of void information can then be achieved by comparing the image captured by the AR device and images in the database. Once the image target is captured, void information will be presented to first responders through the AR interface.

Fig. 9 illustrates the relationship between the image plane and virtual object coordinate system (Carmigniani and Furht 2011). It consists of three transformations that are the object-to-world (**O**), world-to-camera (**C**), and camera-to-image (**P**). ($X_v$, $Y_v$, $Z_v$) is the virtual objects coordinate system, which is the coordinate frame for void information in the virtual world. ($X_w$, $Y_w$, $Z_w$) is the world coordinate frame acting as a global reference for objects in the real world. ($X_c$, $Y_c$, $Z_c$) is the camera coordinate system. This coordinate system locates at the center of the camera and is used to denote the pose of the AR device at any given time. (u, v) is the screen coordinate system in the image plane. Eq. (7) is used to transform from virtual coordinate frame to the camera coordinate frame. The matrix **O** and **C** are both 4×4 transformation matrices that consist of rotation and translation.

$$\begin{bmatrix} X_C \\ Y_C \\ Z_C \\ 1 \end{bmatrix} = \boldsymbol{O}_{4\times 4}\boldsymbol{C}_{4\times 4}\begin{bmatrix} X_w \\ Y_w \\ Z_w \\ 1 \end{bmatrix} \quad (7)$$

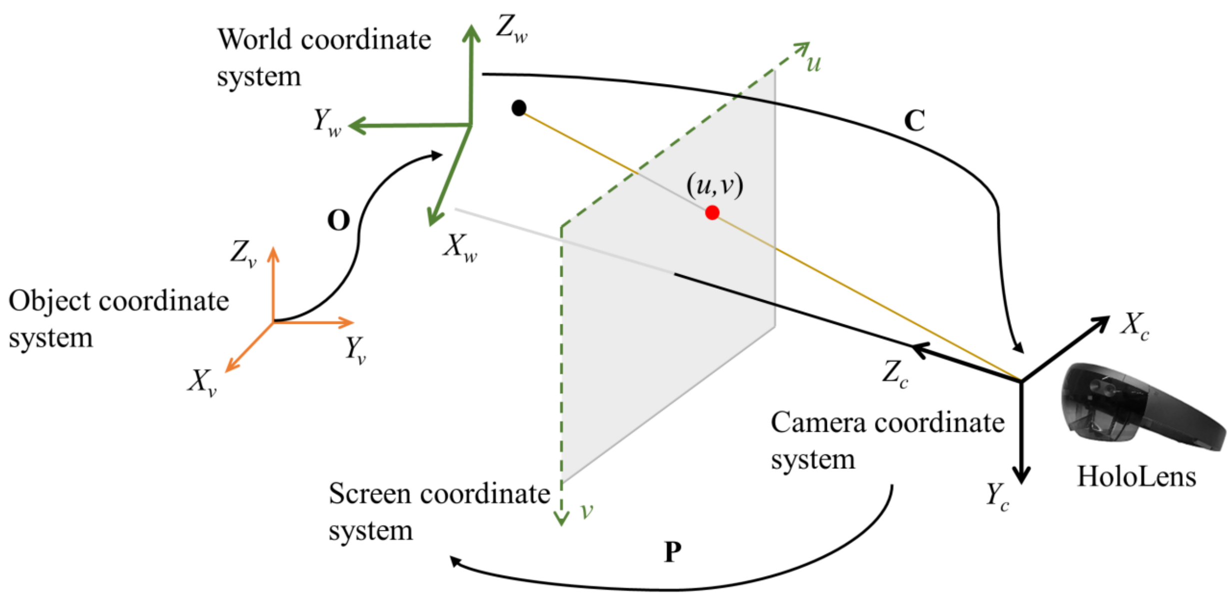


**Fig. 9**. Coordinate transformation between virtual object and image plane

The screen coordinate can then be calculated by Eq. (8), where ($u$, $v$) is the coordinate of the screen coordinate system. $\lambda$ is free scaling parameter; $k_u$ and $k_v$ represent the scale factor relating pixels to distance; $f$ is the focal length; ($c_x$, $c_y$) is the principal point that represents the center of the image. These parameters are intrinsic parameters of the camera.

$$\begin{bmatrix} u \\ v \\ 1 \end{bmatrix} = \lambda \begin{bmatrix} f \times k_u & 0 & c_x \\ 0 & f \times k_v & c_y \\ 0 & 0 & 0 \end{bmatrix} \begin{bmatrix} X_C \\ Y_C \\ Z_C \end{bmatrix} \tag{8}$$

The Vuforia SDK is used to detect and track the image target (PTC 2019). The Vuforia SDK has been widely used with robust performance on a variety of hardware such as HoloLens and smartphones (Frantz et al. 2018; de Ravé et al. 2016). The Vuforia SDK detects feature points in target images. The detected features are compared at run time with features in images captured by an AR device. The quality of an image target is evaluated by star rating ranges between 1 and 5 stars. An image target, with rich in detail, good contrast, and no repetitive patterns, has a higher star rating, which is easy to detect and track. Once the image target is detected, the Vuforia engine will track the image and register virtual content into the real environment. The accuracy of the registration is up to natural features detected in the image target.

Fig. 10 presents an illustration of the developed AR interface prototype. The Unity3D is selected as the development platform due to its easy handling of virtual objects. In Unity3D, the 3D void with relevant information and image target for each structural collapse are imported and aligned together. The 3D void model using the proposed reconstruction method is saved in 3D file format obj. The image target created by Vuforia SDK is saved as Unity package. The Unity3D can build applications to the AR devices for different platforms such as Universal Windows Platform (UWP), iOS, and Android. The first responder will carry AR devices such as HoloLens and mobile phones at disaster sites to visualize void information. When the first responder arrives at structural collapses, void information will be presented to them through the AR interface once the image target is detected. The 3D reconstructed void is overlaid on the top of structural collapse with related depth and volume information. The 3D model is placed on the top of the rubble to ensure first responders can visualize the geometry of the reconstructed void.

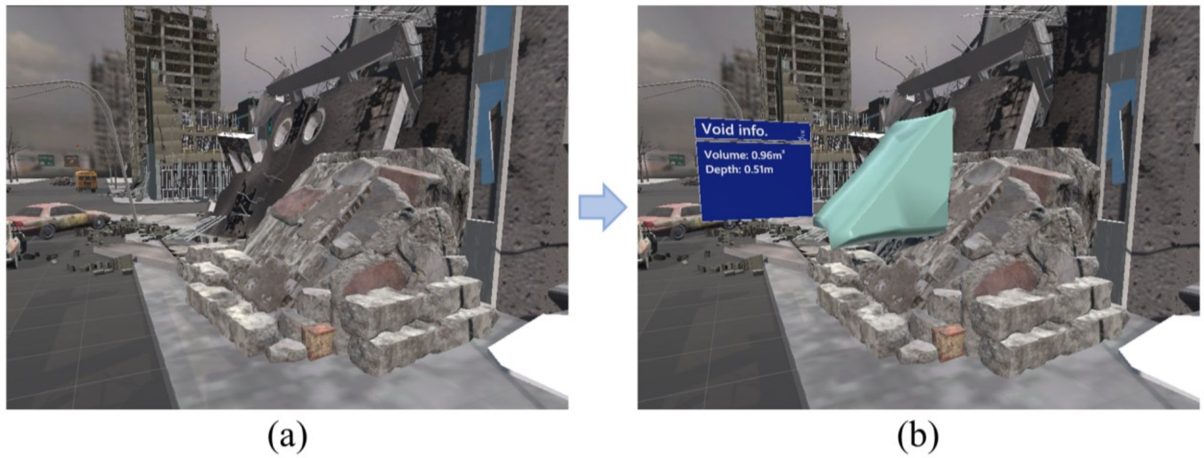


**Fig. 10**. Interface of the AR system prototype: (a) disaster rubbles; and (b) disaster rubbles with void information overlaid

## Experimentation and Evaluation

Two sets of experiments were conducted to validate and evaluate the proposed framework. The first set of experiments aims to evaluate the proposed 3D reconstruction method. The second set of experiments aims to test the applicability of AR in unfavorable conditions that are commonly seen in disaster areas. The experimentation details and results are presented below.

### *Evaluation of 3D Void Reconstruction*

The first set of experiments is conducted to evaluate the efficiency of the proposed 3D reconstruction method. The authors have designed a search and rescue drone to detect voids under the rubble in post-disaster scenarios (Chen et al. 2020). The multirotor drone is equipped with RTK GPS, IMU, camera, and GPR to survey disaster areas. The simulator is used to replicate real disaster scenarios based on photos and videos collected from real disaster sites. With the simulation platform, various disaster scenarios can be arranged for testing and a large amount of GPR data can be collected as in real disaster sites. In addition, large-scale disaster rubbles can be created in the virtual environment which is hard to build in reality. Two lean-to collapse voids were created in the virtual environment. The geometric model of the cross section of the rubble along the GPR scan path is extracted based on UAV trajectory. The synthetic radargram at each cross section is simulated using the gprMax simulator (Warren et al. 2016b). The simulated antenna is set as a 900 MHz Ricker wavelet, which is well accepted. Fig. 11 presents an overview of the two lean-to collapsed voids.

| Scenario | Disaster rubble | Side view | Volume |
|---|---|---|---|
| I | 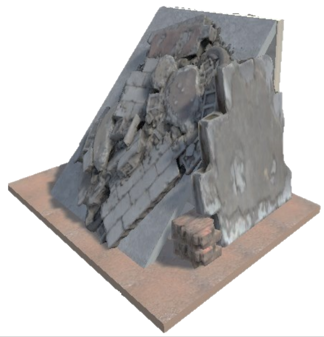 | 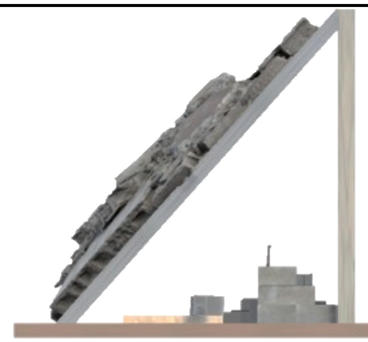 | 8.72m$^3$ |
| II | 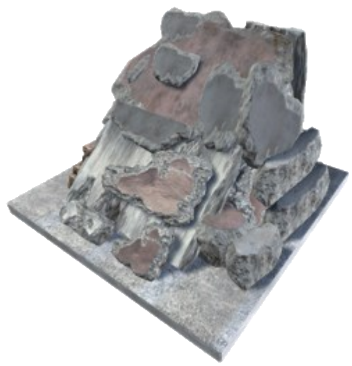 |  | 4.42m$^3$ |

**Fig. 11.** Experimental scenarios of collapsed structures

Fig. 12 presents the results of 3D void reconstruction on the two simulated cases. The UAV flies along the slope of the lean-to collapse structures to collect GPR data. Four GPR scans are collected in both scenarios, where scan paths are approximately parallel to each other. The GPR scan spacing for the collapsed rubble is selected based on the size of collapse and site conditions. The scan spacings for scenario I and scenario II are 0.8m and 0.6m, respectively. The volume of reconstructed void for scenario I is 4.33m$^3$, which is smaller than the ground-truth volume of the void. The underestimate of void volume can be attributed to two reasons. First, the irregular surface will change the transmitting path of EM waves, and thus estimated boundary coordinates are not aligned well with the ground-truth void boundary. Second, there are only four GPR scans for each rubble which cannot capture the full image of the buried void. Increasing the number of scans can better reconstruct void space but at the expense of data collecting and processing time. The estimated buried depth of the void is 0.23m. The ground-truth depth of void varies from 0.13m to 0.55m. The estimated depth is within the range of the ground-truth depth. For Scenario II, the volume of the reconstructed void is 3.80m$^3$, which is close to ground-truth volume. The estimated buried depth of void is 0.18m, which is in agreement with ground-truth depth (0.13m to 0.29m).

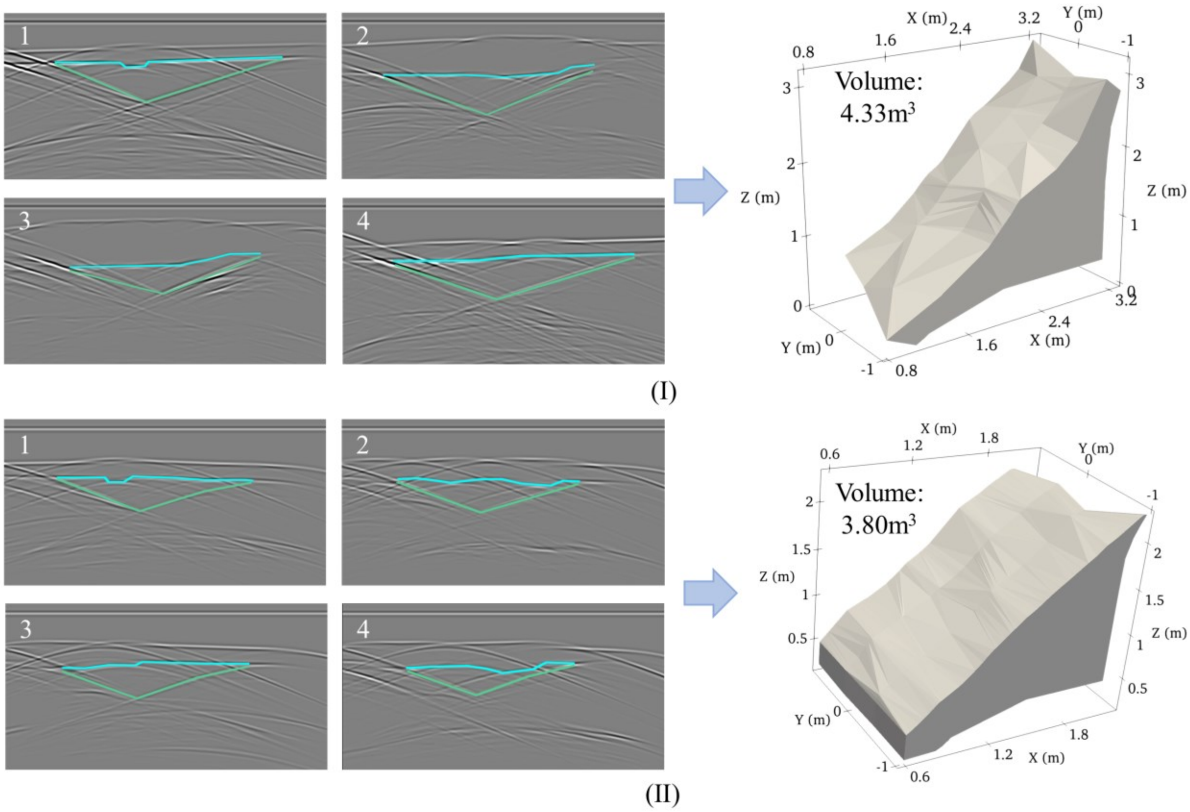


**Fig. 12.** Void reconstruction for simulated scenario I and II

A real experiment is also conducted to validate the proposed 3D reconstruction method. Given that GPR data from recent disasters were not available, a simplified model is built based on the lean-to collapse void with a smaller scale as shown in Fig. 13. The built lean-to collapse normally happens when floor structure fails on one side and the other side is still connected to the wall structure. The wood plate is used to simulate a simplified case of the collapsed floor. It should be noted that the built lean-to collapse is a relatively ideal scenario that can be much more complex in real disaster sites. The aim here is to show the feasibility of the void reconstruction method to reconstruct invisible void space using real GPR scans. The volume of the built lean-to void is around 0.58m$^3$ without considering small objects inside the void space.

The thickness of the wood plate is 5cm. The GPR with a 2GHz antenna was used to collect GPR data. The volume of the reconstructed void is $0.50 m^3$, which is close to the real volume of the void. The estimated void depth is 4.3cm, which is consistent with ground-truth depth. These results demonstrate the feasibility of the proposed reconstruction method using GPR data and justify the pursuit of larger-scale testing in the field.

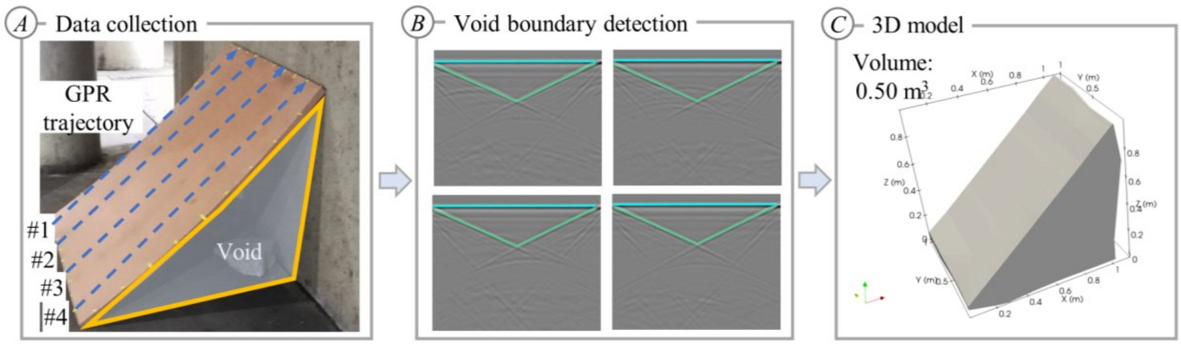


**Fig. 13**. Void reconstruction for the real experiment: (a) data collection; (b) void boundary detection; and (c) 3D model

***Evaluation of the AR System***

The second set of experiments evaluates the efficiency of the AR system. The iPhone 11 with iOS 14.4.2 operating system is selected as the AR device in the evaluation. Note that the developed system can also be adapted to other devices like HoloLens and Android devices. The tracking time is used as a quantitative metric to assess the performance of the AR system. The tracking time is the processing time required to register virtual content into the real world. A small processing time promotes the visualization of void information in a timely manner and improves the user experience. If there is a significant amount of processing time, first responders may fail to capture the void under the rubble. This is because that first responder may move to other places if void information is not visible through the AR device in a short time. Therefore, tracking time is very important for the successful deployment of the AR system. The amount of time is related to the number of detected natural features that can be affected by occlusion and lighting conditions. If nature features cannot be detected or the number of detected features is very small, the void information cannot be registered and visualized by first responders. Hence, the impacts of occlusion and illumination factors on the processing time of the AR system are investigated.

Fig. 14 shows the visualization of reconstructed void overlaid on the abovementioned three collapse scenarios. The results indicate that void can be correctly registered to the structural collapses and be visualized through AR device. Note that since the scenarios I and II are built in the simulation platform, the scene from a first-person perspective is first extracted from the simulator. Then, void information is overlaid on the image and visualized through the AR device. As indicated in Fig. 14, the interaction with the AR system is intuitive, and presented information is easy to understand. This can help reduce the cognitive and information overload of first responders during search and rescue missions.

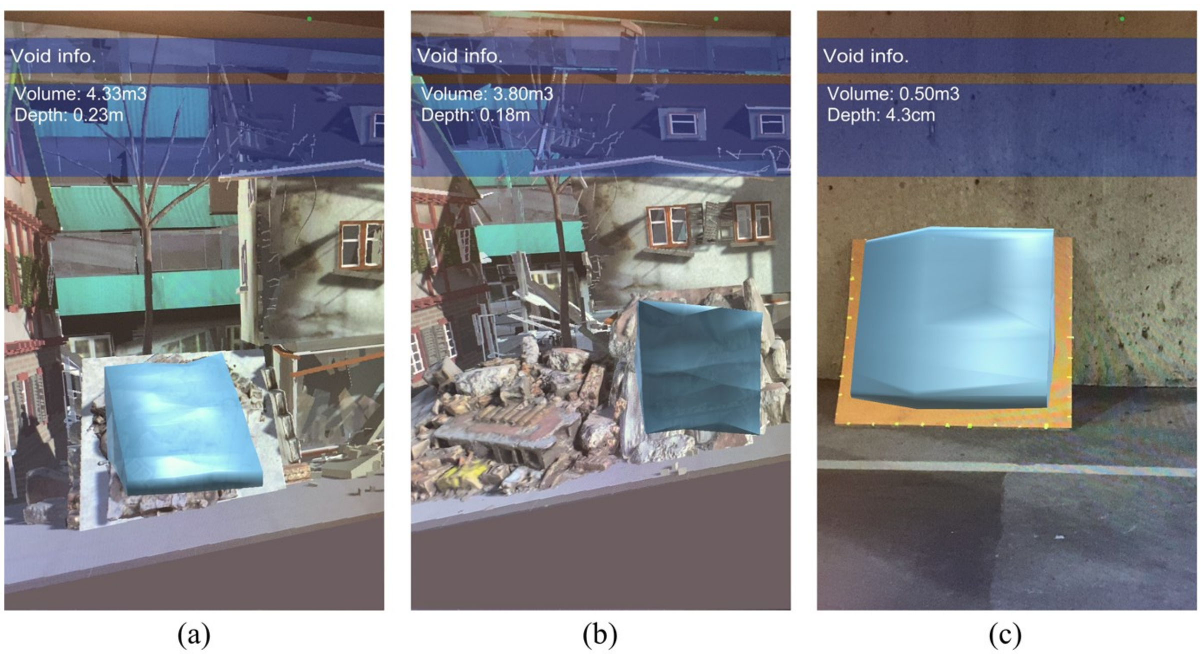


**Fig. 14**. AR visualization of void information: (a) scenario I; (b) scenario II; and (c) real experiment

In order to evaluate the efficiency of the AR system under occlusion and illumination variations, a total number of 34 structural collapses with a potential void underneath were collected and their corresponding surface rubble images were extracted. These surface rubble images were used as image targets to test the AR system. Fig. 15 presents an illustration of the exposure and occlusion settings using the simulated scenario I. The exposure values (EVs) and occlusion percentages are simulated to model possible site conditions. At disaster sites, scene can be occluded due to the dynamics including human and equipment movement and debris removal. In addition, the illumination conditions can be affected by weather and the physical environment at disaster sites.

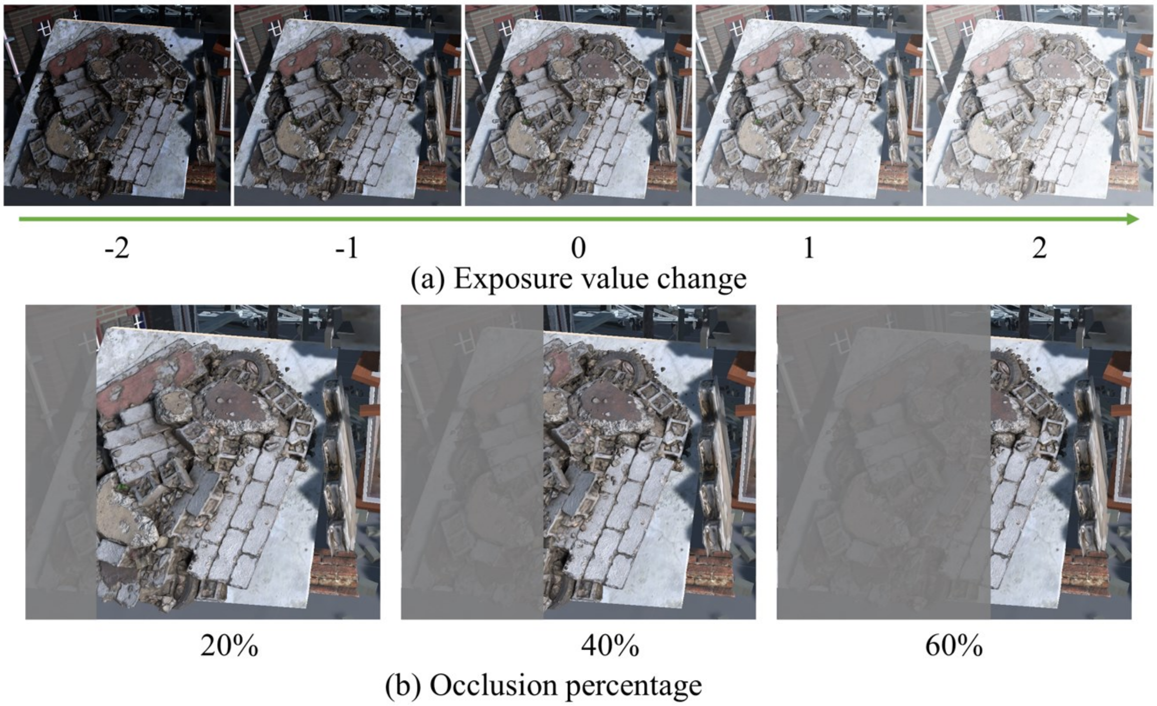


**Fig. 15**. Illustration of exposure value and occlusion percentage settings: (a) exposure value; and (b) occlusion percentage

Fig. 16 (a) indicates the relationship between tracking time and EVs for the 34 investigated collapses. Positive and negative values represent the increased and decreased level of EV from the original EV of the image, respectively. A decreased level of EV represents a darker scene. The results suggest that average tracking time ranges from 0.33 to 0.35s when changes of EV are -2, -1, 0, and 1. Under these scenarios, images of disaster scenes can be easily recognized and tracked in a timely manner. However, when the EV value increases by 2, the tracking time increases significantly compared to that of the original images. Furthermore, eleven images cannot be recognized and tracked in this situation. It indicates that the AR system may not be able to work properly under the extremely bright scene.

Fig. 16 (b) is the tracking time variation with different occlusion percentages which represents the proportion of the hidden part of the image. We investigated the AR system performance with occlusion percentages of 20%, 40%, and 60%. As indicated in Fig. 16 (b), average tacking times are 0.36 and 0.39 for occlusion 20% and 40%, respectively. The system can perform well under low occlusion. Furthermore, average tracking times increase with increasing occlusion percentages. The AR system experiences a significant tracking time increase from occlusion 40% to 60%. In addition, seven images are not recognized for occlusion 60%. It indicates the AR system performance is compromised under the high occlusion. The results demonstrated the reliability and efficiency of the AR system under adverse situations other than extremely bright and high occlusion scenes.

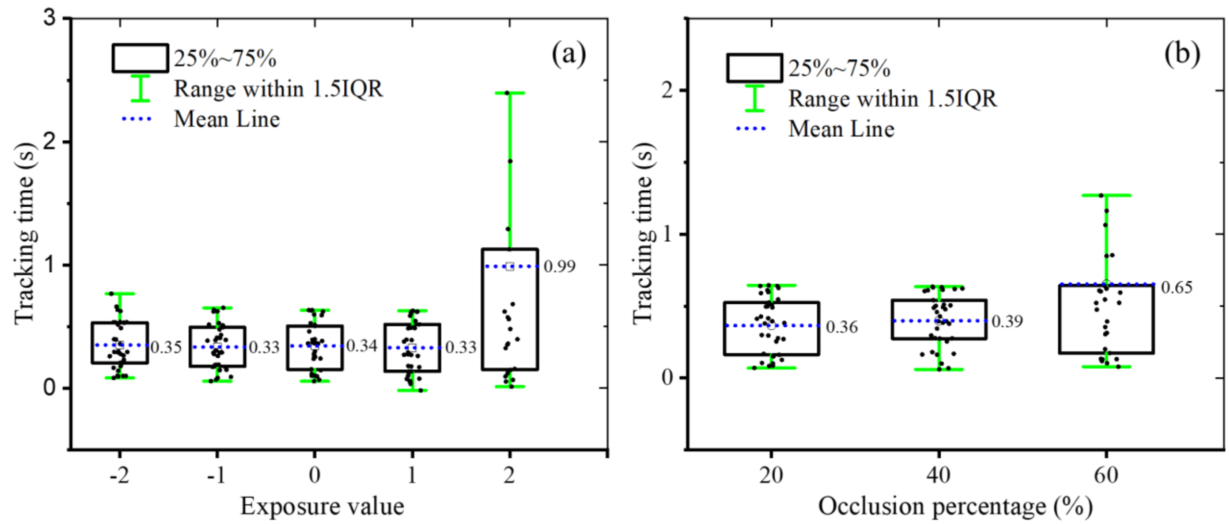


**Fig. 16**. Tracking time variation with exposure value and occlusion: a) exposure value; and (b) occlusion percentage

## Discussion

### *Feasibility of the framework*

The proposed 3D reconstruction method was tested in two simulated and one real experiments. The simulated experiments built relatively large-scale structural collapses with debris and rubbles. 900MHz GPR antenna is used in the simulation. The real experiment built a small-scale lean-to collapse with rubbles in void. The GPR data were collected using 2GHz antenna due to the small scale. The 3D reconstruction method is demonstrated to be feasible to reconstruct void in structural collapses. In all three cases, the estimated void depth is found to be in good agreement with ground-truth void depth. The volume of reconstructed void is found to be smaller than the ground-truth volume of void. This underestimate stems from the error in boundary coordinates estimation and the limited number of GPR scans. In the next step of research, the optimal number and path of GPR scans for void reconstruction will be investigated. The proposed method is suitable for GPR data with different frequencies, which gives more flexibility to first responders in GPR system selection. The low-frequency GPR has a high penetration depth but a low resolution. For large structural collapses, a low-frequency antenna is recommended to ensure entire subsurface structures can be detected in GPR scans. Note that, the low-frequency antenna will reduce the resolution, which could potentially lead to incorrect boundary estimation. On the other hand, a high-frequency antenna is recommended for small-scale structural collapses.

The AR system was developed to register reconstructed void and its related information to the structural collapses in this study. Tracking time was used to evaluate the performance of the AR system. The developed AR interface is found to be effective in overlying void information on structural collapses under dynamic occlusion and lighting conditions. The results indicate that the average tracking time is less than 0.4s for occlusion percentages 20%, 40%, and 60%. In addition, the processing time is less than 0.4s for exposure values -2, -1, 0, and 1. Thus, the proposed AR system is applicable to the dynamic and complex environment at disaster sites. In addition to void information, the system can also integrate other actionable information collected from different sensors. For instance, RGB and depth images were used together to discover access holes in disaster rubbles (Kong et al. 2016). First responders can extricate entrapped victims through access holes, or deploy robots to further explore inside the rubbles. In another example, the thermal camera was used to localize victims on the surface in low-visibility conditions at disaster sites (Doroodgar et al. 2014). The weight of hardware is also acceptable for first responders. For instance, cell phones are generally less than 200 grams and easily accessible. The weight of the HoloLens is around 579 grams. In addition, the HoloLens is easy to use and hands-free, allowing first responders to carry out search and rescue operations while wearing it.

*Applicability of the boundary coordinates extraction method*

In this section, we conducted GPR survey on a scaled experiment and simulated collapsed building structures to investigate the applicability of the proposed boundary coordinates extraction approach. Due to difficulties in conducting validated experiments at disaster sites, we have conducted a scaled experiment in our laboratory using the brick wall. A lean-to collapse void was built (see Fig. 17) and scanned along the slope using the GPR with a 2GHz antenna.

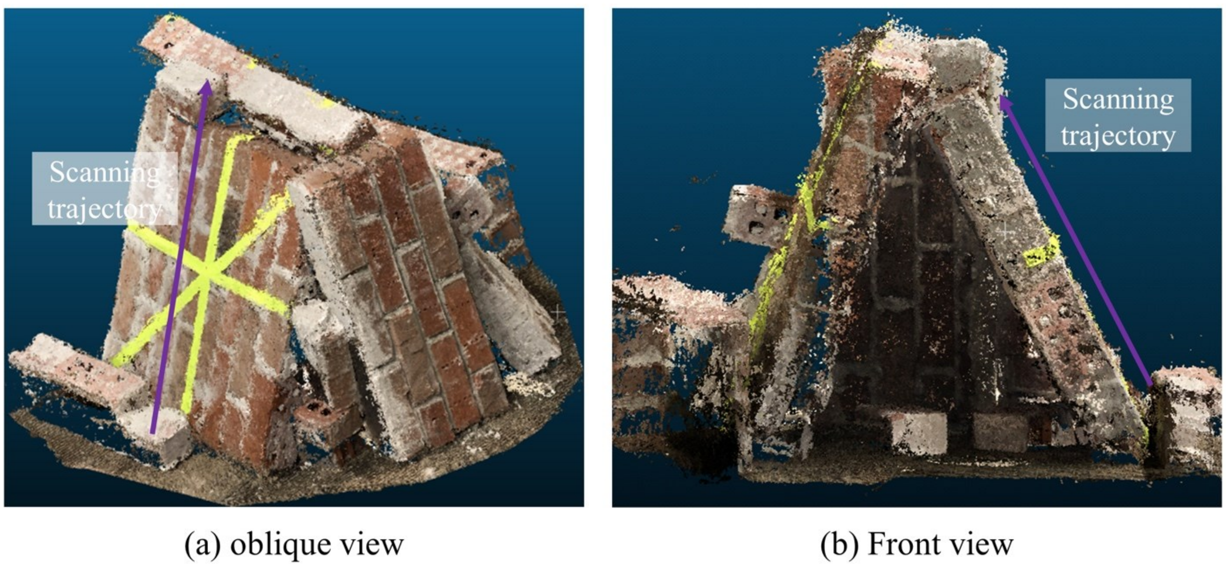


**Fig. 17**. Lean-to collapse built with brick wall: (a) oblique view; and (b) front view

Furthermore, A multi-storey apartment building collapse was simulated using the collapse simulator developed in (Walte and Kostack 2017). The area with potential lean-to collapse void is selected for the GPR survey. The cross section of lean-to collapse is fed into the gprMax simulator to generate the synthetic radargram. Fig. 18 shows the collapsed structure and cross section of a lean-to collapse void.

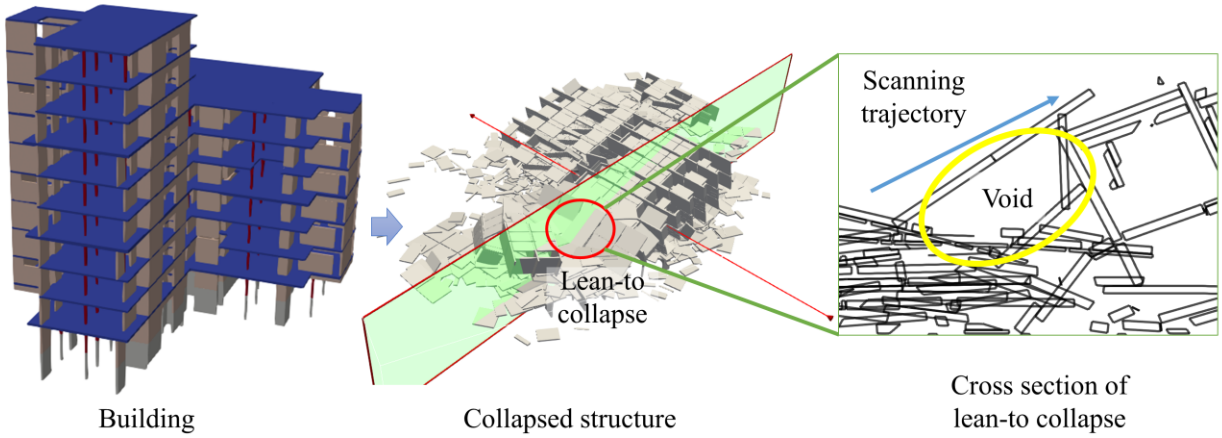


**Fig. 18**. Simulated collapse structure and cross section of lean-to collapse void

Fig. 19 shows the estimation of boundary coordinates for the lean-to collapses. The results indicate that the boundary with strong reflections in the radargram can be identified with the processes of edge detection and binarization. The user can further fine-tune the void boundary based on the binarized boundary. The estimated boundary coordinates are in good agreement with the ground-truth void shape in a 2D space. The results demonstrate the feasibility of the proposed boundary coordinates estimation approach. A combination of multiple GPR scans along the lean-to collapse can reconstruct the void in a 3D space.

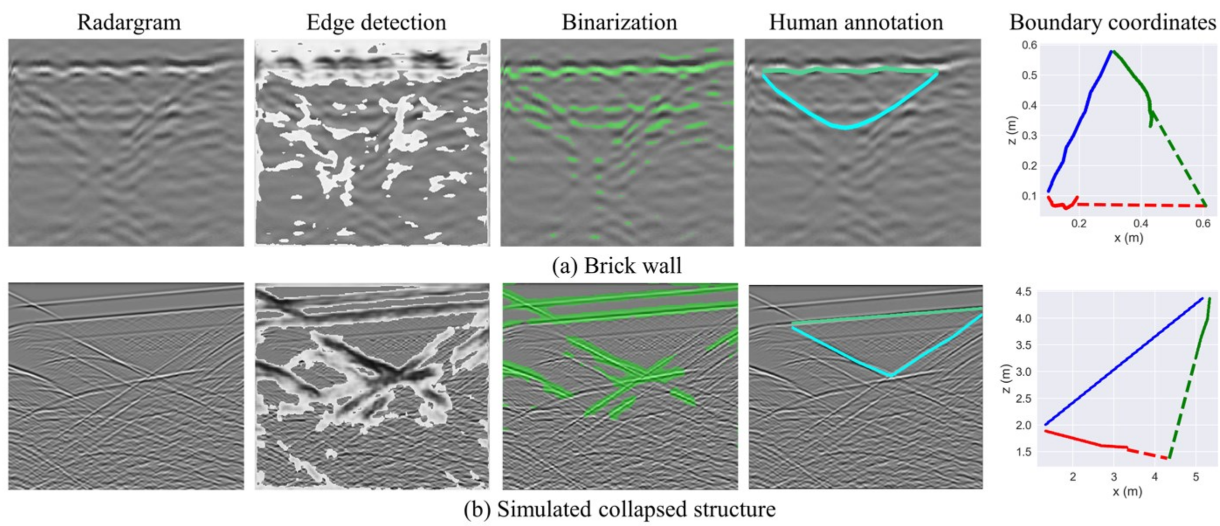


**Fig. 19**. Boundary coordinates estimation for the lean-to collapse built using brick walls and in the simulated collapsed structures: (a) brick wall; and (b) simulated collapse structure

*Limitation and future studies*

This study also has several limitations. First, more information can be acquired from the aboveground and belowground information, thus providing more actionable information through the interface. In the future, the potential correlation between aboveground and belowground information needs to be explored. For example, aboveground information such as building materials can be used to calibrate the GPR. In addition, the predicted subsurface scenarios can be used to determine the GPR scanning trajectory and facilitate the interpretation of GPR data. Second, as a pilot study to demonstrate the feasibility of GPR-based 3D void reconstruction in disaster rubbles, experimental scenarios for void reconstruction in this study were established as relatively simple lean-to collapse voids. In real disaster sites, building collapse could be much more complex for structural collapse with reinforcement steel and heterogenous rubbles, which may compromise the effectiveness of void detection from GPR data. In future studies, field experiments need to be conducted with more realistic scenarios, and advanced processing methods are needed.

Third, the relative permittivity of collapsed structures is estimated based on the material type in our analysis, which could lead to inaccurate depth estimation of void spaces. Conventional relative permittivity estimation approaches such as target burying and common mid-point offset (CMP) are not applicable for complex disaster sites. In the future, more advanced equipment and methods are needed to accurately measure the relative permittivity of collapsed structures in the field.  Fourth, the developed framework is not able to provide information regarding objects and trapped victims in the void, which is critical information for first responders to designate an appropriate search plan. Deep learning-based methods provide possibilities to extract more information from GPR scans if a large GPR dataset at disaster sites becomes available. Furthermore, GPR combined with other sensors such as cameras and rescue radar can generate more data and enable a more comprehensive understanding of subsurface conditions. Finally, the latency of the AR application still requires further improvement. In the future, algorithms should be developed to reduce the time for image detection and tracking under adverse environments such as extremely bright scenes.

## Conclusions

The success of searching and rescuing victims trapped in disaster rubbles primarily depends on the first responders' situational awareness regarding the interior spaces in collapsed structures. To improve first responders' situational awareness, the proposed framework entails two innovations: GPR-based 3D void reconstruction and AR-based information communication that collectively enables the first responders to see through complex and heterogeneous disaster rubbles for efficient, effective, and safe search and rescue. It was found that GPR has great potential for sensing the interior spaces of disaster rubble, and detecting possible void spaces by integrating automatic GPR data processing with human interpretations. The modeling of GPR scanning trajectories and signatures of voids could help the estimation of coordinates of void boundaries to generate sparse 3D point clouds of the detected voids. An improved weighted alpha shape algorithm was also shown to be effective in reconstructing the void spaces in 3D to extract detailed information including depth, size, and geometry for search and rescue operations. The AR-based see-through interface relies on the robust registration of reconstructed interior voids to the exterior surface on disaster sites via image-based matching. Although unfavorable lighting conditions and occlusions could possibly affect the AR performance in terms of average tracking time, the simulations and pilot experimentations demonstrated the potential and feasibility of the AR-based interface. Therefore, the proposed framework and developed methods provide an innovative attempt and technical insights for improving first responders' situational awareness during the urban search and rescue.

## Data Availability Statements

All data, models, or codes that support the findings of this study are provided by the corresponding author upon reasonable request.

## Acknowledgements

This research was funded by the National Science Foundation (NSF) via Grant 1850008, 2129003, and the Tennessee Department of Transportation (TDOT) via the Research Project RES2021-05: "Drones and

Other Technologies to Assist in Disaster Relief Efforts". The authors gratefully acknowledge the support from NSF and TDOT. Any opinions, findings, conclusions, and recommendations expressed in this paper are those of the authors and do not necessarily reflect the views of NSF, TDOT, The University of Tennessee, Knoxville, Loughborough University, The University of Florida, and The University of Texas at San Antonio.

**Appendix A**

Fig. 20 shows the schematic diagram of GPR wave propagation through medium 1 to medium 2. The GPR signal spreads in a medium in a spherical shape. When an EM wave reaches an interface, some of it is reflected and some of it is transmitted across the interface. EM wave can undergo critical refractions, which occurs when the incident angle is such that the refracted wave propagates along with the interface. The critical angle is defined in Eq. (9), where $V_1$ and $V_2$ represent the wave velocity in medium 1 and medium 2 respectively.

$$sin\theta_c = \frac{V_1}{V_2} \tag{9}$$

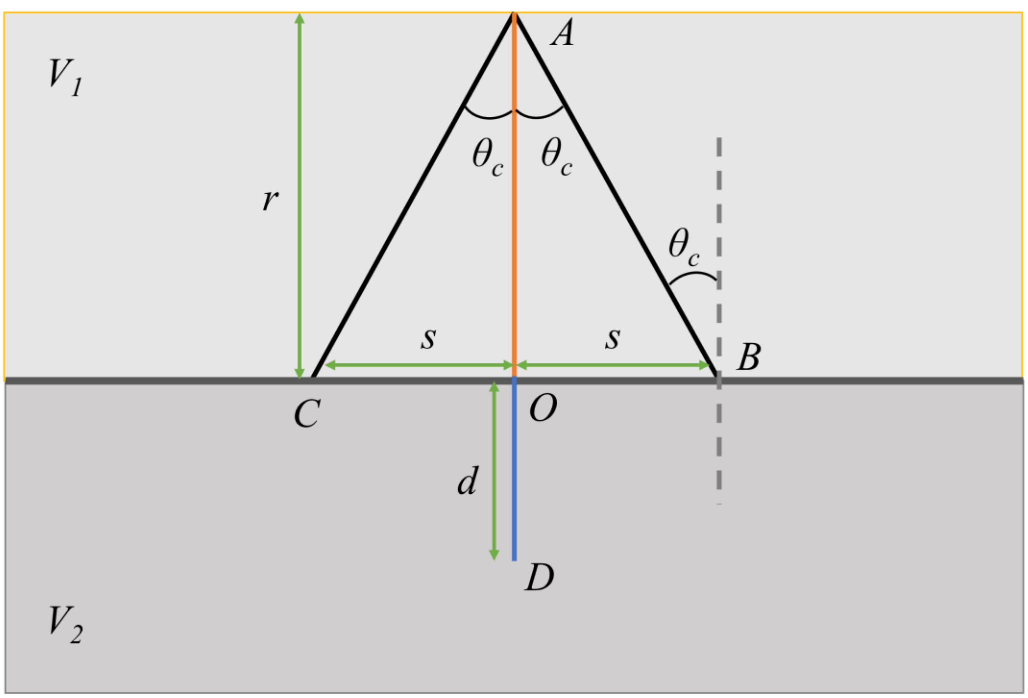


**Fig. 20**. Schematic diagram of EM wave propagates through medium 1 to medium 2

Since EM wave spreads in a spherical shape, the wave path AO, which is perpendicular to the interface, should arrive first. The path AB is the incident wave with a critical angle. The travel time difference between AB and AO can be calculated in Eq. (10)

$$t = \frac{r\left(\frac{1}{cos\theta_c}-1\right)}{V_1} \tag{10}$$

The travel distance *d* for the refracted wave of AO in medium 2 is calculated in Eq. (11)

$$d = \frac{r\left(\frac{1}{cos\theta_c}-1\right)}{V_1}V_2 \tag{11}$$

The three points B, C, and D should form a cycle when transmitting in medium 2, since the wave transmits in a spherical shape. The point O is assumed to be the center of the circles, which leads to *d* equals to *s*. It is defined in Eq. (12).

$$d = s \Rightarrow \frac{r\left(\frac{1}{cos\theta_c}-1\right)}{V_1}V_2 = rtan\theta_c \tag{12}$$

Eq. (12) can be reformulated as Eq. (13)

$$\frac{V_2 - V_1 sin\theta_c}{cos\theta_c} = V_2 \tag{13}$$

Substituting Eq. (9) into Eq. (13) results in Eq. (14). When $V_2 >> V_1$, the equation holds.

$$\frac{2V_2}{V_1^2+V_2^2} = \frac{1}{V_2} \tag{14}$$

**References**


Aboudourib, A., Serhir, M., and Lesselier, D. (2019). “3D reconstruction of tree roots under heterogeneous soil conditions using Ground Penetrating Radar.” *10th International Workshop on Advanced Ground Penetrating Radar*, European Association of Geoscientists & Engineers, 1–6.

Al-Tamimi, M. S. H., Sulong, G., and Shuaib, I. L. (2015). “Alpha shape theory for 3D visualization and volumetric measurement of brain tumor progression using magnetic resonance images.” *Magnetic resonance imaging*, Elsevier, 33(6), 787–803.

Alyassin, A. M., Lancaster, J. L., Downs III, J. H., and Fox, P. T. (1994). “Evaluation of new algorithms for the interactive measurement of surface area and volume.” *Medical physics*, Wiley Online

Library, 21(6), 741–752.

Bacim, F., Ragan, E. D., Stinson, C., Scerbo, S., and Bowman, D. A. (2012). "Collaborative navigation in virtual search and rescue." *IEEE Symposium on 3D User Interfaces 2012, 3DUI 2012 - Proceedings*, IEEE, 187–188.

Bloch, T., Sacks, R., and Rabinovitch, O. (2016). "Interior models of earthquake damaged buildings for search and rescue." *Advanced Engineering Informatics*, Elsevier, 30(1), 65–76.

Burian, F., Zalud, L., Kocmanova, P., Jilek, T., Kopecny, & L., and Kopecny, L. (2014). "Multi-robot system for disaster area exploration." *WIT Transactions on Ecology and the Environment*, 184, 263–274.

Cai, J., Jeon, J., Cai, H., and Li, S. (2020). "Fusing Heterogeneous Information for Underground Utility Map Generation Based on Dempster-Shafer Theory." *Journal of Computing in Civil Engineering*, American Society of Civil Engineers (ASCE), 34(3), 04020013.

Campos, A., Correia, N., Romão, T., Nunes, I., and Simões-Marques, M. (2019). "Mobile augmented reality techniques for emergency response." *Proceedings of the 16th EAI International Conference on Mobile and Ubiquitous Systems: Computing, Networking and Services*, 31–39.

Carmigniani, J., and Furht, B. (2011). "Augmented reality: an overview." *Handbook of augmented reality*, Springer, 3–46.

Chen, J., Li, S., Liu, D., and Li, X. (2020). "AiRobSim: Simulating a Multisensor Aerial Robot for Urban Search and Rescue Operation and Training." *Sensors*, MDPI AG, 20(18), 5223.

Cist, D. B. (2009). "Non-destructive evaluation after destruction: using ground penetrating radar for search and rescue." *7th International Symposium on Non-Destructive Testing in Civil Engineering, Nantes, France, Expanded Abstracts*, Citeseer.

Coovert, M. D., Lee, T., Shindev, I., and Sun, Y. (2014). "Spatial augmented reality as a method for a mobile robot to communicate intended movement." *Computers in Human Behavior*, Elsevier, 34, 241–248.

Couch, S. R. (2008). *Handbook of Disaster Research*. *Contemporary Sociology: A Journal of Reviews*, Handbooks of Sociology and Social Research, (H. Rodríguez, W. Donner, and J. E. Trainor, eds.), Springer International Publishing, Cham.

Doroodgar, B., Liu, Y., and Nejat, G. (2014). "A learning-based semi-autonomous controller for robotic exploration of unknown disaster scenes while searching for victims." *IEEE Transactions on Cybernetics*, Institute of Electrical and Electronics Engineers Inc., 44(12), 2168–2267.

Frantz, T., Jansen, B., Duerinck, J., and Vandemeulebroucke, J. (2018). "Augmenting Microsoft's HoloLens with vuforia tracking for neuronavigation." *Healthcare Technology Letters*, 5(5), 221–225.

Fruehauf, F., Heilig, A., Schneebeli, M., Fellin, W., and Scherzer, O. (2009). "Experiments and algorithms to detect snow avalanche victims using airborne ground-penetrating radar." *IEEE Transactions on Geoscience and Remote Sensing*, 47(7), 2240–2251.

Gianni, M., Gonnelli, G., Sinha, A., Menna, M., and Pirri, F. (2013). "An Augmented Reality approach for trajectory planning and control of tracked vehicles in rescue environments." *2013 IEEE International Symposium on Safety, Security, and Rescue Robotics, SSRR 2013*.

Gomes, L., Bellon, O. R. P., and Silva, L. (2014). "3D reconstruction methods for digital preservation of cultural heritage: A survey." *Pattern Recognition Letters*, Elsevier, 50, 3–14.

Hajebi, K., Abbasi-Yadkori, Y., Shahbazi, H., and Zhang, H. (2011). "Fast approximate nearest-neighbor search with k-nearest neighbor graph." *Twenty-Second International Joint Conference on Artificial Intelligence*.

Heilig, A., Schneebeli, M., and Fellin, W. (2008). "Feasibility study of a system for airborne detection of avalanche victims with ground penetrating radar and a possible automatic location algorithm." *Cold Regions Science and Technology*, Elsevier, 51(2–3), 178–190.

Hu, D., Hou, F., Blakely, J., and Li, S. (2020a). "Augmented Reality Based Visualization for Concrete Bridge Deck Deterioration Characterized by Ground Penetrating Radar." *Construction Research Congress 2020: Computer Applications - Selected Papers from the Construction Research Congress 2020*, 1156–1164.

Hu, D., Hou, F., and Li, S. (2020b). “Ground-penetrating radar-based root architecture detection and characterization.” *18th International Conference on Ground Penetrating Radar*, 243–246.

Hu, D., Li, S., Chen, J., and Kamat, V. R. (2019). “Detecting, locating, and characterizing voids in disaster rubble for search and rescue.” *Advanced Engineering Informatics*, 42.

Koester, C. (2018). “We Must Change the Statistics of Confined Space Injuries and Fatalities -- Occupational Health & Safety.” *Occupational Health and Safety*, <https://ohsonline.com/articles/2018/08/01/we-must-change-the-statistics-of-confined-space-injuries-and-fatalities.aspx> (Feb. 22, 2019).

Kong, C., Ferworn, A., Coleshill, E., Tran, J., and Derpanis, K. G. (2016). “What is a Hole? Discovering Access Holes in Disaster Rubble with Functional and Photometric Attributes.” *Journal of Field Robotics*, John Wiley & Sons, Ltd, 33(6), 825–836.

Levatti, H. U., Prat Catalán, P., Ledesma Villalba, A., Cuadrado Cabello, A., and Cordero Arias, J. A. (2017). “Experimental analysis of 3D cracking in drying soils using ground-penetrating radar.” *Geotechnical Testing Journal*, 40(2), 1–23.

Li, H., Chou, C., Fan, L., Li, B., Wang, D., and Song, D. (2020). “Toward Automatic Subsurface Pipeline Mapping by Fusing a Ground-Penetrating Radar and a Camera.” *IEEE Transactions on Automation Science and Engineering*, Institute of Electrical and Electronics Engineers Inc., 17(2), 722–734.

Li, S., Cai, H., and Kamat, V. R. (2015). “Uncertainty-aware geospatial system for mapping and visualizing underground utilities.” *Automation in Construction*, Elsevier, 53, 105–119.

Liu, H., Chen, Z., Lu, H., Han, F., Liu, C., Li, J., and Cui, J. (2020a). “Migration of ground penetrating radar with antenna radiation pattern correction.” *IEEE Geoscience and Remote Sensing Letters*, IEEE.

Liu, L., Liu, Z., Xie, H., Barrowes, B., and Bagtzoglou, A. C. (2014). “Numerical simulation of UWB impulse radar vital sign detection at an earthquake disaster site.” *Ad Hoc Networks*, Elsevier, 13(PART A), 34–41.

Liu, X., Chen, J., Butnor, J. R., Qin, G., Cui, X., Fan, B., Lin, H., and Guo, L. (2020b). “Noninvasive 2D and 3D mapping of root zone soil moisture through the detection of coarse roots with ground-penetrating radar." *Water Resources Research*, Wiley Online Library, 56(5), e2019WR026930.

Murphy, R. R., Casper, J., and Micire, M. (2001). "Potential Tasks and Research Issues for Mobile Robots in RoboCup Rescue." Springer, Berlin, Heidelberg, 339–344.

Nadkarni, P. (2016). "Core Technologies: Data Mining and 'Big Data.'" *Clinical Research Computing*, Elsevier, 187–204.

Núñez-Nieto, X., Solla, M., Novo, A., and Lorenzo, H. (2014). "Three-dimensional ground-penetrating radar methodologies for the characterization and volumetric reconstruction of underground tunneling." *Construction and Building Materials journal*, Elsevier, 71, 551–560.

Otsu, N. (1979). "A threshold selection method from gray-level histograms." *IEEE transactions on systems, man, and cybernetics*, IEEE, 9(1), 62–66.

Poteyeva, M., Denver, M., Barsky, L. E., and Aguirre, B. E. (2007). "Search and Rescue Activities in Disasters." Springer, New York, NY, 200–216.

PTC. (2019). "Industrial Augmented Reality - Vuforia." <https://www.ptc.com/en/products/augmented-reality> (Aug. 28, 2019).

de Ravé, E. G., Jiménez-Hornero, F. J., Ariza-Villaverde, A. B., Taguas-Ruiz, J., Gutiérrez De Ravé, E., Jiménez-Hornero, F. J., Ariza-Villaverde, & A. B., Taguas-Ruiz, & J., de Ravé, E. G., Jiménez-Hornero, F. J., Ariza-Villaverde, A. B., and Taguas-Ruiz, J. (2016). "DiedricAR: a mobile augmented reality system designed for the ubiquitous descriptive geometry learning." *Multimedia Tools and Applications*, 75(16), 9641–9663.

Reardon, C., Lee, K., and Fink, J. (2018). "Come See This! Augmented Reality to Enable Human-Robot Cooperative Search." *2018 IEEE International Symposium on Safety, Security, and Rescue Robotics, SSRR 2018*.

Tong, Z., Gao, J., and Zhang, H. (2017). "Recognition, location, measurement, and 3D reconstruction of concealed cracks using convolutional neural networks." *Construction and Building Materials*, Elsevier, 146, 775–787.

Vassell, M., Apperson, O., Calyam, P., Gillis, J., and Ahmad, S. (2016). "Intelligent Dashboard for augmented reality based incident command response co-ordination." *2016 13th IEEE Annual Consumer Communications & Networking Conference (CCNC)*, IEEE, 976–979.

Walte, O., and Kostack, K. (2017). *Blender and Bullet physics engine based on fast on-site assessment tool*. Uusimaa.

Wang, R., Lu, H., Xiao, J., Li, Y., and Qiu, Q. (2018). "The Design of an Augmented Reality System for Urban Search and Rescue." *2018 International Conference on Intelligence and Safety for Robotics, ISR 2018*, <https://ieeexplore.ieee.org/stamp/stamp.jsp?arnumber=8535823> (Dec. 19, 2019).

Wani, A. R., Shabir, S., and Naaz, R. (2013). "Augmented reality for fire & emergency services." *Int. Conf. on Recent Trends in Communication and Computer Networks*, 32–41.

Warren, C., Giannopoulos, A., and Giannakis, I. (2016a). "gprMax: Open source software to simulate electromagnetic wave propagation for Ground Penetrating Radar." *Computer Physics Communications*, Elsevier B.V., 209, 163–170.

Warren, C., Giannopoulos, A., and Giannakis, I. (2016b). "gprMax: Open source software to simulate electromagnetic wave propagation for Ground Penetrating Radar." *Computer Physics Communications*, North-Holland, 209, 163–170.

Wibisono, J. K., and Hang, H.-M. (2021). "Fined: Fast Inference Network for Edge Detection." *2021 IEEE International Conference on Multimedia and Expo (ICME)*, 1–6.

Yan, K., Wu, S., and Fang, G. (2021). "Detection of Quasi-Static Trapped Human Being Using Mono-Static UWB Life-Detection Radar." *Applied Sciences 2021, Vol. 11, Page 3129*, Multidisciplinary Digital Publishing Institute, 11(7), 3129.

Yang, D., Zhu, Z., and Liang, B. (2019). "Vital Sign Signal Extraction Method Based on Permutation Entropy and EEMD Algorithm for Ultra-Wideband Radar." *IEEE Access*, Institute of Electrical and Electronics Engineers Inc., 7, 178879–178890.

Yuan, C., Li, S., Cai, H., and Kamat, V. R. (2018). "GPR Signature Detection and Decomposition for Mapping Buried Utilities with Complex Spatial Configuration." *Journal of Computing in Civil*

*Engineering*, 32(4), 04018026.

Zhang, W., and Hoorfar, A. (2019). “MIMO Ground Penetrating Radar Imaging Through Multilayered Subsurface Using Total Variation Minimization.” *IEEE Transactions on Geoscience and Remote Sensing*, Institute of Electrical and Electronics Engineers Inc., 57(4), 2107–2115.

Zhekov, S. S., Franek, O., and Pedersen, G. F. (2020). “Dielectric properties of common building materials for ultrawideband propagation studies [measurements corner].” *IEEE Antennas and Propagation Magazine*, IEEE, 62(1), 72–81.